PHYSICAL REVIEW A VOLUME 35, NUMBER 4 FEBRUARY 15, 1987

Competition between amplified spontaneous emission and the four-wave-mixing process

Robert W. Boyd, Michelle S. Malcuit, and Daniel J. Gauthier
The Institute of Optics, University of Rochester, Rochester, New York 14627

Kazimierz Rzążewski
Institute for Theoretical Physics, Polish Academy of Sciences, 02-668 Warsaw, Al. Lotnikow 32/46, Poland
(Received 22 September 1986)

Competition between amplified spontaneous emission (ASE) and the four-wave-mixing (FWM) process has been observed under conditions of two-photon resonant excitation of the sodium $3d$ level. The nature of the competition is that the FWM process is able to prevent the occurrence of ASE, even though the gain of the ASE process calculated in the absence of competition effects is much larger than that of FWM. The ASE is suppressed because the fields generated by the FWM process create a new excitation pathway connecting the ground and $3d$ levels, and under quite general conditions this pathway interferes destructively with that due solely to the applied laser field. These effects are modeled theoretically by solving perturbatively the density-matrix equations of the atomic system, thereby determining the population in the upper level and the nonlinear polarization of the medium. The coupling between the various optical fields due to the nonlinear polarization is described by coupled amplitude equations. The solution to these equations predicts that when the wave-vector mismatch is not too large the fields evolve spatially to reach steady-state values, and that the population excited to the $3d$ level by the total steady-state optical field is much smaller than that due to the incident laser field alone. We have observed experimentally the suppression of ASE by FWM and have observed that this suppression does not occur when the medium is excited with counterpropagating beams that cannot efficiently excite the FWM process. In addition, we have conducted a series of experiments that shows that the degree of suppression of ASE depends on the intensity and focusing characteristics of the incident laser as expected on the basis of our theoretical model.

I. INTRODUCTION

An interesting possibility that can occur in nonlinear optics is the competition between two different processes in a complex and highly nonlinear manner. Perhaps the simplest example of competition effects in nonlinear optics is competition between two different stimulated scattering processes.[1] The nature of the competition in this case is that the process with the largest gain grows most rapidly, thus robbing the pump wave of its energy and preventing the growth of other processes. A more subtle type of competition is that in which a coherent (that is, phase-matched) nonlinear optical process suppresses an incoherent nonlinear optical process. The first reported example of such an interaction was the suppression of multiphoton ionization by third-harmonic generation in an atomic vapor.[2,3] Several additional theoretical and experimental studies[3–8] of competition effects involving these processes have subsequently been reported.

We recently reported the observation of another example of competition between a coherent and an incoherent nonlinear optical process, namely the suppression of amplified spontaneous emission (ASE) by the four-wave-mixing (FWM) process.[9] Previous theories of competition effects would not have predicted that competition would occur under our experimental conditions in which the only resonant interaction involves a two-photon transition. We interpreted out observations theoretically by means of a density-matrix calculation performed within a semiclassical framework. This calculation shows that the ASE is suppressed due to a destructive interference between two excitation pathways connecting the ground and excited states. A similar calculation in which the electromagnetic field is treated quantum mechanically has recently been reported by Agarwal.[10] His calculation shows that, under conditions of suppression of ASE, the fields generated by the FWM process constitute a squeezed state of the radiation field. The primary intent of the present paper is to present a more detailed account of the experimental and theoretical work presented in our previous letter,[9] and to examine the conditions under which strong suppression is expected to occur.

The experiment in which we observed competition between FWM and ASE was performed in atomic sodium vapor.[9] An intense laser field of frequency ω_1 is tuned near to the $3s \rightarrow 3d$ two-photon-allowed transition, as shown in Fig. 1(a). Four-wave mixing[11–22] can then occur, leading to the generation of two new fields, one at frequency ω_2 which is close to the $3d \rightarrow 3p$ transition frequency and the other at frequency $\omega_3 = 2\omega_1 - \omega_2$ which is close to the $3p \rightarrow 3s$ transition frequency. When the laser is tuned exactly to the two-photon-allowed transition, population can be transferred to the $3d$ level, inverting it with respect to the $3p$ level and leading to ASE (Refs. 23 and 24) at the $3d \rightarrow 3p$ transition frequency, as shown in Fig. 1(b). We are able to distinguish these two processes because they display different experimental signatures. Due to phase-matching considerations, the FWM signal is emitted only in the forward direction and, for the sodium

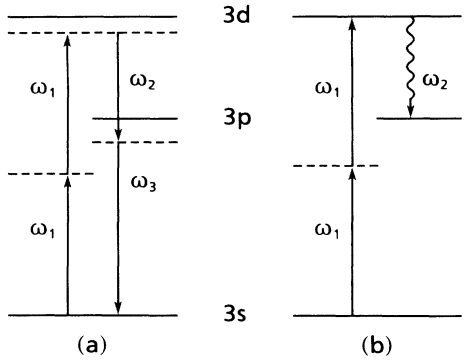

FIG. 1. Under conditions of two-photon-resonant excitatior of the sodium $3d$ level by an incident laser field of frequency ω_1 either (a) the four-wave-mixing (FWM) process or (b) amplified spontaneous emission (ASE) can occur. Competition between these two processes has been observed.

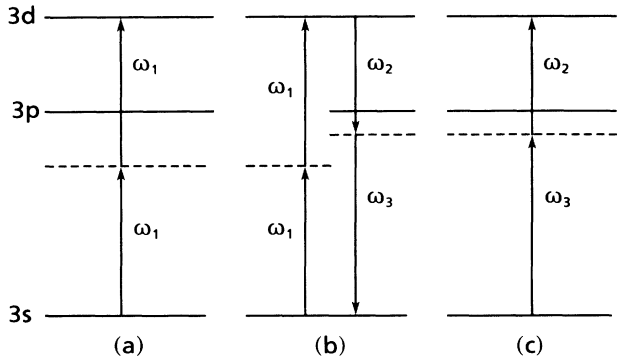

FIG. 2. The nature of the suppression of the upper-level population by the FWM process is illustrated. (a) The incident laser field creates an excitation pathway connecting the ground and excited states. (b) Due to the FWM process, fields at frequencies ω_2 and ω_3 are generated. (c) These new fields create a second excitation pathway connecting these levels. Under quite general conditions, this pathway interferes destructively with that due to the incident field.

number densities used in the experiment, is emitted in the form of a cone surrounding the transmitted laser beam. In contrast, the ASE signal is emitted in both the forward and backward directions because it is a pure gain process. Furthermore, the FWM process leads to a much broader output spectrum because it involves a virtual intermediate level. Since the ASE process involves the excitation of a real as opposed to a virtual level, one would expect that this process would have a larger gain than the FWM process. In fact, the gain for ASE under our experimental conditions calculated in the absence of competition effects is $\sim 10^4$ cm^{-2}, whereas the gain for the FWM process calculated under the same conditions is ~ 100 cm^{-1}, as will be shown below. However, experimentally we observe a strong FWM signal and little if any ASE. Other nonlinear optical processes such as hyper-Raman scattering were much weaker than either of these processes under any of our experimental conditions.

We have performed an additional experiment which shows that the ASE signal is absent because the FWM process actually suppresses the ASE process. We excite the sodium vapor with two counterpropagating laser fields of different frequencies, adjusted so that the sum of their frequencies is equal to the $3s \rightarrow 3d$ transition frequency and so that the sum of their intensities is equal to that used in the experiment using a single laser field in which the ASE signal was absent. In the new experiment, the FWM process is not phase matched and cannot occur efficiently. In this case a strong bidirectional ASE signal is observed.

These experimental results are perhaps at first sight surprising because it is not clear how a coherent (i.e., phase-matched) process such as FWM can suppress an incoherent process such as ASE which requires only a population inversion. The origin of the competition between these processes is illustrated in Fig. 2. Since only the laser field of frequency ω_1 is incident on the sodium cell, initially two-photon absorption involving two laser photons [Fig. 2(a)] is the only excitation pathway connecting the ground and excited states. However, FWM leads to the generation of new frequency components of frequency ω_2 and ω_3, as shown in Fig. 2(b). These new fields create a second pathway of excitation of the $3d$ level, involving two-photon absorption of an ω_2 and an ω_3 photon, as shown in Fig. 2(c). We will show in the theoretical section of this paper that under a broad range of experimental conditions the two new fields are generated with amplitudes and phases adjusted in such a manner that these two pathways interfere destructively, preventing the excitation of the $3d$ level. Any process such as ASE that requires the presence of population in the two-photon excited level will thereby be suppressed. In particular, the efficiency of multiphoton ionization[2] and of parametric mixing[25] can be degraded, as can the possibility of achieving a population inversion in laser-pumped lasers.[26]

II. THEORY

In this section we present a theoretical treatment of the suppression of the upper-level population due to the FWM process. We first solve to fourth order in perturbation theory the density-matrix equations of motion for the three-level atomic system, shown in Fig. 3, in the presence of the incident and generated fields. We use the results of this calculation to determine the population in the upper level and to determine the nonlinear polarization of the medium and hence to derive coupled amplitude for the three interacting fields. We then study the nature of the solution to these equations and find that if the wave-vector mismatch is not too large the fields evolve spatially to reach steady-state values, and that in the presence of this steady-state field the upper-level population is at least partially suppressed. For the case of perfect phase matching, complete suppression of the upper-level population is

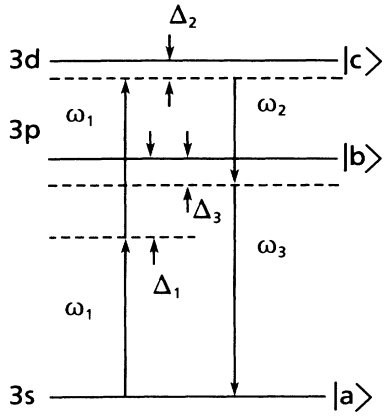

FIG. 3. Energy-level diagram showing the FWM process and the notation used in the calculation.

predicted. The vanishing of the upper-level population can be traced to a destructive interference between two pathways connecting the ground and excited states.

A. Density-matrix calculation

We assume that the field incident on the atomic vapor can be represented as

$$E(z,t)=\sum_j \tilde{E}_j e^{-i\omega_j t}+\text{c.c.},\quad j=1,2,3 \tag{1a}$$

where

$$\tilde{E}_j=E_j e^{ik_j z}, \tag{1b}$$

and that the atomic response is governed by the density-matrix equations of motion which we take to be of the form[27,28]

$$\dot{\rho}_{ll}=-\sum_{(W_i<W_l)}\gamma_{li}\rho_{ll}+\sum_{(W_i>W_l)}\gamma_{il}\rho_{ii}+\frac{i}{\hbar}\sum_i(\mu_{li}\rho_{il}-\mu_{il}\rho_{li})E(t) \tag{2a}$$

and

$$\dot{\rho}_{lm}=-(i\omega_{lm}+\Gamma_{lm})\rho_{lm}+\frac{i}{\hbar}\sum_i(\mu_{li}\rho_{im}-\mu_{im}\rho_{li})E(t)\quad (l\neq m), \tag{2b}$$

where W_i denotes the energy of level i. We further assume that the density-matrix elements can be expanded in a perturbation series of the form

$$\rho_{lm}=\rho_{lm}^{(0)}+\rho_{lm}^{(1)}+\rho_{lm}^{(2)}+\rho_{lm}^{(3)}+\cdots, \tag{3}$$

and that the unperturbed density matrix can be represented as

$$\rho_{aa}^{(0)}=1 \tag{4a}$$

and

$$\rho_{lm}^{(0)}=0\ \ (\text{for } l\neq m \text{ and for } l=m\neq a). \tag{4b}$$

In solving the density-matrix equations, we retain only those terms that contribute to the two-photon resonant response of the atom. In lowest order of perturbation theory, these contributions are those that remain in the rotating-wave approximation, and in this approximation the first-order correction to the density matrix is given as

$$\rho_{ba}^{(1)}=\frac{\mu_{ba}}{\hbar}\left[\frac{\tilde{E}_1 e^{-i\omega_1 t}}{\Delta_1-i\Gamma_{ba}}+\frac{\tilde{E}_2 e^{-i\omega_2 t}}{2\Delta_1-\Delta_3-i\Gamma_{ba}}+\frac{\tilde{E}_3 e^{-i\omega_3 t}}{\Delta_3-i\Gamma_{ba}}\right], \tag{5}$$

where $\Delta_1=\omega_{ba}-\omega_1$, $\Delta_2=\omega_{ca}-2\omega_1$, and $\Delta_3=\omega_{ba}-\omega_3$, with $\omega_{ij}=(W_i-W_j)/\hbar$. The second-order contribution to the density matrix is given by

$$\rho_{ca}^{(2)}=\frac{\mu_{cb}\mu_{ba}}{\hbar^2}\left[\frac{\tilde{E}_1^{\,2}e^{-i2\omega_1 t}}{(\Delta_1-i\Gamma_{ba})(\Delta_2-i\Gamma_{ca})}+\frac{\tilde{E}_2\tilde{E}_3 e^{-i(\omega_2+\omega_3)t}}{(2\Delta_1-\Delta_3-i\Gamma_{ba})(\Delta_2-i\Gamma_{ca})}+\frac{\tilde{E}_2\tilde{E}_3 e^{-i(\omega_2+\omega_3)t}}{(\Delta_3-i\Gamma_{ba})(\Delta_2-i\Gamma_{ca})}\right]. \tag{6}$$

We assume that none of the applied fields can resonantly excite the $b\rightarrow a$ transition, that is, that Δ_1, Δ_3, and $2\Delta_1-\Delta_3$ are much greater than Γ_{ba}, so that $\rho_{bb}^{(2)}$ is negligible. In the next order of perturbation theory, there exists two off-diagonal elements of the density matrix which represent the nonlinear polarization of the medium. These density-matrix elements are given by

$$\begin{aligned}\rho_{cb}^{(3)}=-\frac{|\mu_{ba}|^2\mu_{cb}}{(\Delta_2-i\Gamma_{ca})\hbar^3}\Bigg[&\frac{|\tilde{E}_1|^2\tilde{E}_1 e^{-i\omega_1 t}}{(\Delta_1-i\Gamma_{ba})(\Delta_2-\Delta_1-i\Gamma_{cb})}+\frac{\tilde{E}_1^{\,2}\tilde{E}_2^{\,*}e^{-i\omega_3 t}}{(\Delta_1-i\Gamma_{ba})(\Delta_2+\Delta_3-2\Delta_1-i\Gamma_{cb})}+\frac{\tilde{E}_1^{\,2}\tilde{E}_3^{\,*}e^{-i\omega_2 t}}{(\Delta_1-i\Gamma_{ba})(\Delta_2-\Delta_3-i\Gamma_{cb})}\\&+\frac{\tilde{E}_2\tilde{E}_3\tilde{E}_1^{\,*}e^{-i\omega_1 t}}{(2\Delta_1-\Delta_3-i\Gamma_{ba})(\Delta_2-\Delta_1-i\Gamma_{cb})}+\frac{|\tilde{E}_2|^2\tilde{E}_3 e^{-i\omega_3 t}}{(2\Delta_1-\Delta_3-i\Gamma_{ba})(\Delta_2+\Delta_3-2\Delta_1-i\Gamma_{cb})}\\&+\frac{|\tilde{E}_3|^2\tilde{E}_2 e^{-i\omega_2 t}}{(2\Delta_1-\Delta_3-i\Gamma_{ba})(\Delta_2-\Delta_3-i\Gamma_{cb})}+\frac{\tilde{E}_3\tilde{E}_2\tilde{E}_1^{\,*}e^{-i\omega_1 t}}{(\Delta_3-i\Gamma_{ba})(\Delta_2-\Delta_1-i\Gamma_{cb})}\\&+\frac{|\tilde{E}_2|^2\tilde{E}_3 e^{-i\omega_3 t}}{(\Delta_3-i\Gamma_{ba})(\Delta_2+\Delta_3-2\Delta_1-i\Gamma_{cb})}+\frac{|\tilde{E}_3|^2\tilde{E}_2 e^{-i\omega_2 t}}{(\Delta_3-i\Gamma_{ba})(\Delta_2-\Delta_3-i\Gamma_{cb})}\Bigg],\end{aligned} \tag{7a}$$

and

$$\rho_{ba}^{(3)}=\frac{|\mu_{cb}|^2\mu_{ba}}{(\Delta_2-i\Gamma_{ca})\hbar^3}\left[\frac{|\tilde{E}_1|^2\tilde{E}_1e^{-i\omega_1 t}}{(\Delta_1-i\Gamma_{ba})^2}+\frac{\tilde{E}_1^2\tilde{E}_2^*e^{-i\omega_3 t}}{(\Delta_1-i\Gamma_{ba})(\Delta_3-i\Gamma_{ba})}+\frac{\tilde{E}_1^2\tilde{E}_3^*e^{-i\omega_2 t}}{(\Delta_1-i\Gamma_{ba})(2\Delta_1-\Delta_3-i\Gamma_{ba})}\right.$$
$$+\frac{\tilde{E}_2\tilde{E}_3\tilde{E}_1^*e^{-i\omega_1 t}}{(2\Delta_1-\Delta_3-i\Gamma_{ba})(\Delta_1-i\Gamma_{ba})}+\frac{|\tilde{E}_2|^2\tilde{E}_3e^{-i\omega_3 t}}{(2\Delta_1-\Delta_3-i\Gamma_{ba})(\Delta_3-i\Gamma_{ba})}+\frac{|\tilde{E}_3|^2\tilde{E}_2e^{-i\omega_2 t}}{(2\Delta_1-\Delta_3-i\Gamma_{ba})^2}$$
$$\left.+\frac{\tilde{E}_3\tilde{E}_2\tilde{E}_1^*e^{-i\omega_1 t}}{(\Delta_3-i\Gamma_{ba})(\Delta_1-i\Gamma_{ba})}+\frac{|\tilde{E}_2|^2\tilde{E}_3e^{-i\omega_3 t}}{(\Delta_3-i\Gamma_{ba})^2}+\frac{|\tilde{E}_3|^2\tilde{E}_2e^{-i\omega_2 t}}{(\Delta_3-i\Gamma_{ba})(2\Delta_1-\Delta_3-i\Gamma_{cb})}\right]. \tag{7b}$$

Finally, to fourth order in perturbation theory, we obtain an expression for the population in the upper level c as

$$\rho_{cc}^{(4)}=-\frac{2|\mu_{ba}|^2|\mu_{cb}|^2}{\hbar^4\gamma_c}$$
$$\times\mathrm{Im}\left\{\frac{1}{\Delta_2-i\Gamma_{ca}}\left[\frac{|\tilde{E}_1|^4}{(\Delta_1-i\Gamma_{ba})(\Delta_2-\Delta_1-i\Gamma_{cb})}\right.\right.$$
$$+\tilde{E}_1^2\tilde{E}_2^*\tilde{E}_3^*\left[\frac{1}{(\Delta_1-i\Gamma_{ba})(\Delta_2+\Delta_3-2\Delta_1-i\Gamma_{cb})}+\frac{1}{(\Delta_1-i\Gamma_{ba})(\Delta_2-\Delta_3-i\Gamma_{cb})}\right]$$
$$+\tilde{E}_1^{*2}\tilde{E}_2\tilde{E}_3\left[\frac{1}{(2\Delta_1-\Delta_3-i\Gamma_{ba})(\Delta_2-\Delta_1-i\Gamma_{cb})}+\frac{1}{(\Delta_3-i\Gamma_{ba})(\Delta_2-\Delta_1-i\Gamma_{cb})}\right]$$
$$+|\tilde{E}_2|^2|\tilde{E}_3|^2\left[\frac{1}{(2\Delta_1-\Delta_3-i\Gamma_{ba})(\Delta_2+\Delta_3-2\Delta_1-i\Gamma_{cb})}\right.$$
$$+\frac{1}{(2\Delta_1-\Delta_3-i\Gamma_{ba})(\Delta_2-\Delta_3-i\Gamma_{cb})}$$
$$\left.\left.\left.+\frac{1}{(\Delta_3-i\Gamma_{ba})(\Delta_2+\Delta_3-2\Delta_1-i\Gamma_{cb})}+\frac{1}{(\Delta_3-i\Gamma_{ba})(\Delta_2-\Delta_3-i\Gamma_{cb})}\right]\right]\right\}, \tag{8a}$$

where

$$\gamma_c=\sum_{\substack{i\\(W_i<W_c)}}\gamma_{ci} \tag{8b}$$

denotes the inverse of the lifetime of level c. Under our approximations, $\rho_{bb}^{(4)}$ is negligible.

B. The nonlinear polarization

The nonlinear polarization of the medium can be obtained in terms of the density matrix calculated in Sec. II A as

$$P(z,t)=N(\mu_{ab}\rho_{ba}^{(3)}+\mu_{bc}\rho_{cb}^{(3)}+\text{c.c.}), \tag{9}$$

where N denotes the atomic number density. It is convenient to represent the nonlinear polarization in terms of its frequency components as

$$P(z,t)=\sum_j P(\omega_j)e^{i(k_jz-\omega_jt)}+\text{c.c.}\quad(j=1,2,3). \tag{10}$$

The quantities $P(\omega_j)$ can be obtained in general from Eqs. (7), (9), and (10). However, our experiments were conducted under conditions such that to good approximation the inequalities

$$\Delta_1\gg\Delta_3\gg\Delta_2\quad\text{and}\quad\Delta_1,\Delta_3\gg\Gamma_{ba} \tag{11}$$

were satisfied. Under these conditions, the nonlinear polarizations can be expressed simply as

$$P(\omega_1)=2\chi^{\mathrm{FWM}}E_2E_3E_1^*e^{-i\Delta kz}+2\chi_s^{\mathrm{TPA}}|E_1|^2E_1, \tag{12a}$$
$$P(\omega_2)=\chi^{\mathrm{FWM}}E_1^2E_3^*e^{+i\Delta kz}+\chi_d^{\mathrm{TPA}}|E_3|^2E_2, \tag{12b}$$
$$P(\omega_3)=\chi^{\mathrm{FWM}}E_1^2E_2^*e^{+i\Delta kz}+\chi_d^{\mathrm{TPA}}|E_2|^2E_3, \tag{12c}$$

where the susceptibilities for FWM and for two-photon

absorption (TPA) involving the same and different frequencies are given by

$$\chi^{\mathrm{FWM}}=\frac{\Delta_1}{\Delta_3}\chi_s^{\mathrm{TPA}}=\frac{\Delta_3}{\Delta_1}\chi_d^{\mathrm{TPA}}=\frac{N\,|\mu_{ba}|^2|\mu_{cb}|^2}{\hbar^3\Delta_1\Delta_3(\Delta_2-i\Gamma_{ca})}\ , \tag{13a}$$

and where the wave-vector mismatch Δk is defined by

$$\Delta k=k_2+k_3-2k_1\ . \tag{13b}$$

The spatial evolution of the field amplitudes are described in the slowly varying amplitude approximation by the coupled amplitude equations

$$\frac{dE_j}{dz}=\frac{2\pi i\omega_j^2}{k_jc^2}P(\omega_j)\ . \tag{14}$$

Through use of these equations, one can determine the variation of the intensity $S_j=(cn_j/2\pi)|E_j|^2$ of each field component as

$$\frac{dS_j}{dz}=-2\omega_j\mathrm{Im}[E_j^*P(\omega_j)]\ . \tag{15}$$

Under these same set of conditions (11), the population in the upper level can be expressed as

$$\rho_{cc}^{(4)}=\frac{2}{\hbar N\gamma_c}[\mathrm{Im}(\chi_s^{\mathrm{TPA}})|E_1|^4+\mathrm{Im}(\chi_d^{\mathrm{TPA}})|E_2|^2|E_3|^2 +\mathrm{Im}(\chi^{\mathrm{FWM}})(E_2E_3E_1^{*2}e^{-i\Delta kz}+\mathrm{c.c.})]\ . \tag{16}$$

This quantity is related to the total intensity $S_{\mathrm{tot}}=S_1+S_2+S_3$ of the optical field through the relation

$$\frac{dS_{\mathrm{tot}}}{dz}=-2N\hbar\omega_1\gamma_c\rho_{cc}^{(4)}\ , \tag{17}$$

which is obtained straightforwardly using Eqs. (12)–(16). Note that the expression (16) for $\rho_{cc}^{(4)}$ contains an interference term which for appropriate values of the complex field amplitudes can cause the population in level c to vanish. This cancellation is the origin of the suppression of ASE by FWM. The origin of this interference can be traced to the expression [Eq. (6)] for the second-order coherence between the ground and upper levels, which under the present conditions reduces to

$$\rho_{ca}^{(2)}=\frac{\hbar\Delta_3}{N\mu_{bc}\mu_{ab}} \times\chi^{\mathrm{FWM}}\left[E_1^2+\frac{\Delta_1}{\Delta_3}E_2E_3e^{-i\Delta kz}\right]e^{i(2k_1z-2\omega_1t)}\ . \tag{18}$$

When the complex field amplitudes obey the condition

$$E_1^2=-\frac{\Delta_1}{\Delta_3}E_2E_3e^{-i\Delta kz}\ , \tag{19}$$

$\rho_{ca}^{(2)}$ vanishes, and consequently all higher-order contributions to the density matrix vanish. In particular, $\rho_{cc}^{(4)}$ vanishes, implying that no population is transferred to the upper level. Furthermore, the nonlinear polarization which is proportional to $\rho_{cb}^{(3)}$ and to $\rho_{ba}^{(3)}$ also vanishes, and hence from Eq. (14) one sees that the field amplitudes remain spatially invariant. In Sec. II C we investigate the nature of the solutions to the coupled amplitude equations (14) and thereby determine the conditions under which propagation causes the fields to evolve so that their amplitudes obey condition (19).

C. The coupled amplitude equations

In order to solve the coupled amplitude equations (14), it is convenient to rewrite them in terms of the real field amplitudes and phases. We express the complex field amplitudes E_j as

$$E_j=A_je^{i\phi_j} \tag{20a}$$

and introduce the phase angle β of the nonlinear susceptibilities (13) as

$$\tan\beta=\frac{\mathrm{Im}i\chi^{\mathrm{FWM}}}{\mathrm{Re}i\chi^{\mathrm{FWM}}}=-\frac{\Delta_2}{\Gamma_{ca}}\ . \tag{20b}$$

In terms of these quantities, the coupled amplitude equations become

$$\frac{dA_1}{dz}=-\alpha_1A_1\left[A_2A_3\cos(\theta+\beta)+\frac{\Delta_3}{\Delta_1}A_1^2\cos\beta\right]\ , \tag{21a}$$

$$\frac{dA_2}{dz}=-\alpha_2A_3\left[A_1^2\cos(\theta-\beta)+\frac{\Delta_1}{\Delta_3}A_2A_3\cos\beta\right]\ , \tag{21b}$$

$$\frac{dA_3}{dz}=-\alpha_3A_2\left[A_1^2\cos(\theta-\beta)+\frac{\Delta_1}{\Delta_3}A_2A_3\cos\beta\right]\ , \tag{21c}$$

where the new phase variable θ is defined by

$$\theta=\phi_2+\phi_3-2\phi_1-\Delta kz \tag{22a}$$

and obeys the equation

$$\frac{d\theta}{dz}=2\alpha_1A_2A_3\sin(\theta+\beta) +\left[\alpha_2\frac{A_1^2A_3}{A_2}+\alpha_3\frac{A_1^2A_2}{A_3}\right]\sin(\theta-\beta) +\left[2\alpha_1\frac{\Delta_3}{\Delta_1}A_1^2-\alpha_2\frac{\Delta_1}{\Delta_3}A_3^2-\alpha_3\frac{\Delta_1}{\Delta_3}A_2^2\right]\sin\beta-\Delta k\ , \tag{22b}$$

with coupling coefficients α_j given by

$$\alpha_1=\frac{4\pi\omega_1^2}{k_1c^2}|\chi^{\mathrm{FWM}}|\ , \tag{23a}$$

$$\alpha_j=\frac{2\pi\omega_j^2}{k_jc^2}|\chi^{\mathrm{FWM}}|\quad(j=2,3)\ . \tag{23b}$$

In terms of the new variables A_j and θ, the population in the upper level is given by

$$\rho_{cc}^{(4)}=\frac{2\mathrm{Im}\chi^{\mathrm{FWM}}}{N\hbar\gamma_c}\frac{\Delta_3}{\Delta_1} \times\left[A_1^4+\left[\frac{\Delta_1}{\Delta_3}\right]^2A_2^2A_3^2+2\frac{\Delta_1}{\Delta_3}A_2A_3A_1^2\cos\theta\right]\ , \tag{24}$$

and the condition for suppression under our experimental conditions where Δ_1 and Δ_3 have the same sign is $\theta=\pi$ and $A_2A_3/A_1^2=\Delta_3/\Delta_1$.

D. Solution for $\Delta_2=0$ and $\Delta k=0$

The set of coupled equations given by Eqs. (21) and (22) are very difficult to solve in general. However, considerable simplification occurs for the special case in which the incident laser is tuned to the two-photon resonance so that $\Delta_2=0$ and hence $\beta=0$ and in which the phase-matching condition is precisely satisfied so that $\Delta k=0$. In this case, Eq. (22b) has the form

$$\frac{d\theta}{dz}=f(z)\sin\theta\ , \tag{25}$$

where $f(z)$ is positive definite. One can see by inspection that the asymptotic solution of this equation for large values of z is $\theta\rightarrow\pi$. Physically, one expects that θ will approach this value after propagation through a distance several times the characteristic coupling distance $\Lambda=(\alpha_2\alpha_3)^{-1/2}A_1^{-2}$. Once θ has approached this value, the coupled equations for the real amplitudes become

$$\frac{dA_1}{dz}=\alpha_1 A_1\left[A_2A_3-\frac{\Delta_3}{\Delta_1}A_1^2\right]\ , \tag{26a}$$

$$\frac{dA_2}{dz}=\alpha_2 A_3\left[A_1^2-\frac{\Delta_1}{\Delta_3}A_2A_3\right]\ , \tag{26b}$$

$$\frac{dA_3}{dz}=\alpha_3 A_2\left[A_1^2-\frac{\Delta_1}{\Delta_3}A_2A_3\right]\ . \tag{26c}$$

These equations possess a steady-state solution in which the field amplitudes are spatially invariant and are related by

$$\frac{A_2A_3}{A_1^2}=\frac{\Delta_3}{\Delta_1}\ . \tag{27}$$

This condition is precisely the condition which according to Eq. (24) leads to the suppression of the upper-level population. In order to determine the conditions under which the fields actually evolve so as to fulfill condition (27), one needs to solve the coupled set of Eqs. (26). This set of equations does not yield a simple analytic solution. However, in our experiments the fractional conversion from the pump wave into the generated waves is always small. In the limit in which one can assume that the pump amplitude A_1 remains constant, the reduced set of Eqs. (26b) and (26c) can readily be solved analytically. One can see by inspection of Eqs. (26b) and (26c) [or for that matter from the more general Eqs. (21b) and (21c)] that the quantity

$$\frac{A_2^2}{\alpha_2}-\frac{A_3^2}{\alpha_3} \tag{28}$$

is a constant of the motion. This fact allows one to represent A_2 in Eq. (26c) as

$$A_2=\left[\frac{\alpha_2}{\alpha_3}(A_3^2-C^2)\right]^{1/2}\ , \tag{29}$$

where C is the constant of integration. The resulting equation is separable and can be directly integrated. The resulting integral can be simplified through use of the substitution

$$A_3=C\cosh x \tag{30}$$

and yields the solution

$$x=\tanh^{-1}\left[\frac{1}{a}\left\{(a^2+b^2)^{1/2}\times\tanh\left[(a^2+b^2)^{1/2}z+\tanh^{-1}\left[\frac{a\tanh x_0+b}{(a^2+b^2)^{1/2}}\right]\right]-b\right\}\right], \tag{31}$$

where x_0 is another constant of integration, $a=(\alpha_2\alpha_3)^{1/2}A_1^2$, and $b=(\alpha_2\Delta_1C^2/2\Delta_3)$. In the limit $z\rightarrow\infty$ the ω_3 field approaches the value

$$A_3\rightarrow A_1\left[\frac{\Delta_3}{\Delta_1}\right]^{1/2}\left[\frac{\alpha_3}{\alpha_2}\right]^{1/4} \tag{32a}$$

and hence, through use of Eq. (29) in the limit $C\rightarrow0$

$$A_2\rightarrow A_1\left[\frac{\Delta_3}{\Delta_1}\right]^{1/2}\left[\frac{\alpha_2}{\alpha_3}\right]^{1/4}\quad\text{as } z\rightarrow\infty\ . \tag{32b}$$

The limit $C\rightarrow0$ is the limit in which the ω_2 and ω_3 fields contain the same number of photons, and hence corresponds to the experimental situation in which these two fields grow from noise. Note that in the limit $C\rightarrow0$, $z\rightarrow\infty$ the product of the asymptotic values of A_2 and A_3 approaches the value $A_1^2\Delta_3/\Delta_1$ as required by Eq. (27) for a steady-state solution and that, according to Eq. (24) with $\theta=\pi$, $\rho_{cc}^{(4)}$ vanishes under these conditions. In Fig. 4

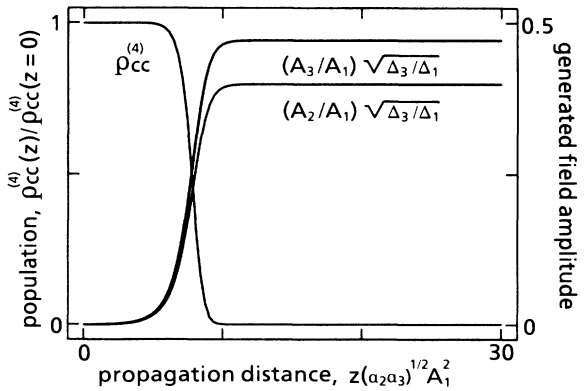

FIG. 4. Spatial evolution of the generated fields A_2 and A_3 and the excited state population $\rho_{cc}^{(4)}$ for the case of perfect phase matching ($\Delta k=0$) and exact tuning to the two-photon resonance ($\Delta_2=0$), as predicted by the theory described in the text.

we show the spatial evolution of A_2 and A_3 as given by Eqs. (29)—(31) for the case in which the constants of integration have the values $x_0=0$ and $C=10^{-5}A_1$. Also shown at each position in the medium is the value of $\rho_{cc}^{(4)}$ calculated from Eq. (24). Note that A_2 and A_3 grow to their steady-state values in several coupling lengths and that the upper-level population is suppressed once the fields have attained these values.

E. Solution of arbitrary Δ_2 and Δk

In the more general case in which Δk and β are arbitrary, it is very difficult to solve the set [(21) and (22)] of coupled equations for the spatial evolution of the fields. However, even in this case we can determine those conditions under which steady-state (spatially uniform) solutions to these equation exist. We do this by setting all of the spatial derivatives to zero and solving the resulting set of equations algebraically. It is easy to show that in general this set of equations does not possess a solution except for special values of Δk and β. However, in the constant pump limit (A_1 and ϕ_1 constant), which is relevant to our experimental conditions, steady-state solutions for the ω_2 and ω_3 fields exist under fairly general conditions. In the constant pump limit the equations that must be solved simultaneously are Eqs. (21b), (21c), and Eq. (22b) with those contributions due to the variation of ϕ_1 (i.e., those which are proportional to α_1) omitted. The condition $dA_2/dz=0$ requires that

$$\frac{A_2A_3}{A_1^2}=\frac{-\Delta_3\cos(\theta-\beta)}{\Delta_1\cos\beta}\ , \tag{33a}$$

as does the condition $dA_3/dz=0$. The condition $d\theta/dz=0$ requires that

$$\sin(\theta-\beta)=\frac{\Delta k+(\alpha_2A_3^2+\alpha_3A_2^2)(\Delta_1/\Delta_3)\sin\beta}{\alpha_2A_3A_1^2/A_2+\alpha_3A_2A_1^2/A_3}\ . \tag{33b}$$

These equations are now solved simultaneously subject to the constraint imposed by Eq. (29) (which is valid in general), where for simplicity we take $C=0$ since it is small compared to the steady-state values of A_1 and A_3 for the case of interest in which the fields grow from noise. We find that θ is given by the equation

$$\sin(\theta-\beta)+\tan\beta\cos(\theta-\beta)=\frac{\Delta k}{2(\alpha_2\alpha_3)^{1/2}A_1^2}\ . \tag{34a}$$

The fields are then given in terms of θ by

$$A_2^2=\frac{\alpha_2}{\alpha_3}A_3^2=-\left[\frac{\alpha_2}{\alpha_3}\right]^{1/2}\frac{\Delta_3A_1^2\cos(\theta-\beta)}{\Delta_1\cos\beta}\ . \tag{34b}$$

The fields and upper-level populations given by Eq. (24) are shown for representative cases in Fig. 5. In Fig. 5(a) we show the relative phase angle θ of the optical fields plotted as a function of the normalized wave-vector mismatch for several different values of the phase angle β characterizing the nonlinearity. Recall that only for $\theta=\pi$ can there be complete suppression of the upper-state population. Each curve is plotted over the entire domain the values of Δk for which a steady-state solution exists. For $\beta\neq0$, this domain includes regions in which a weak input

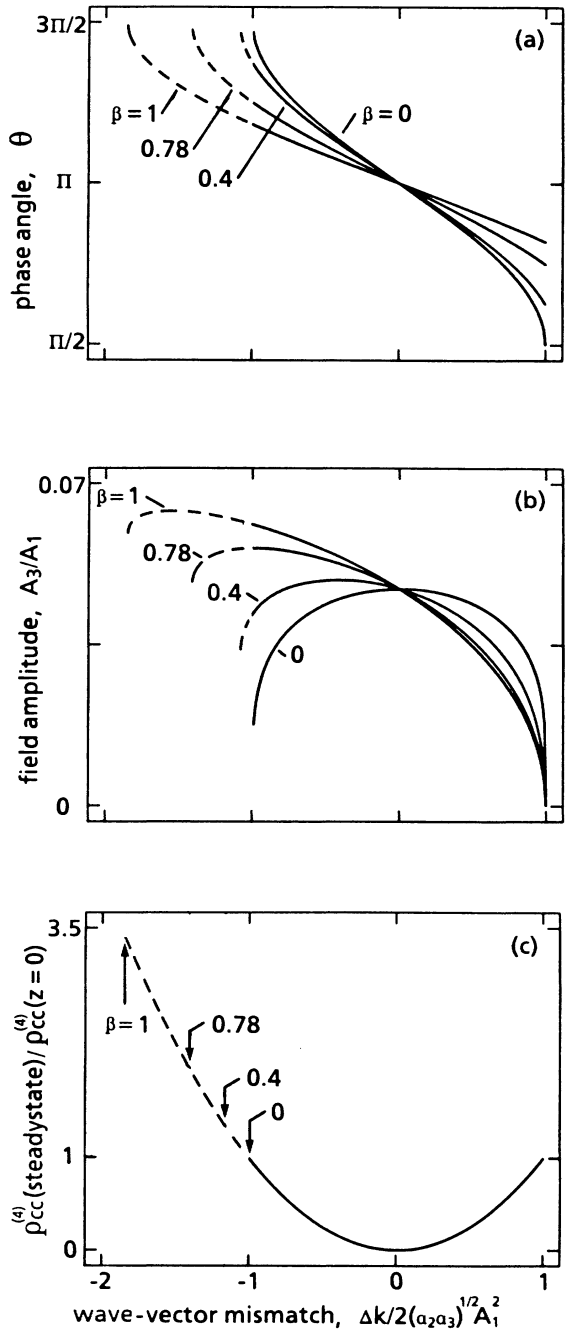

FIG. 5. (a) and (b) Steady-state solutions to the coupled amplitude equations (21) and (22) in the constant-pump limit, plotted as a function of the normalized wave-vector mismatch for several different values of the phase angle β of the nonlinear susceptibility. The solution is plotted over the entire range of values of Δk for which a stable, steady-state solution exists. (c) Upper-level population $\rho_{cc}^{(4)}$ in the presence of the fields shown in (a) and (b), normalized by its value in the presence of the pump field alone. All of these curves lie on top of one another; however, curves corresponding to different values of β have different end points as indicated. The dashed portions of the curves correspond to conditions under which the solution will not grow from noise.

wave will not experience net gain and hence where the steady-state solution cannot be reached by the growth of the generated fields from noise. These regions cannot be realized in an experiment such as ours involving a single input frequency, and thus are shown dashed in the figure. In the limit of large detuning from the two-photon resonance, β approaches the value $\pi/2$ and θ attains the value π everywhere. Figure 5(b) shows the dependence of the field amplitude A_3 on the wave-vector mismatch and on β. According to Eq. (29), the field amplitude A_2 is directly proportional to A_3. Figure 5(c) shows the dependence of the normalized upper-state population on Δk for various values of β. Note that the curves for different values of β lie on top of one another, except that they have different end points within the region where the curves are shown dashed. Curves of the sort shown in Fig. 5 can be obtained for negative values of β by reflecting the curves for positive values of β about the axis $\Delta k=0$. For the conditions of our experiment, Δ_1 and Δ_3 are both positive, and hence, for collinear propagation of the three waves Δk is negative. By allowing the waves to be noncollinear, however, Δk can be made to increase and eventually to take on positive values.

We have been unable to find an analytic solution for the spatial evolution of the fields for the case of arbitrary values of Δ_2 and of Δk, and we have therefore integrated the coupling amplitude equations (14) numerically under these conditions. Representative solutions are shown in Fig. 6. We have assumed the values $\Delta_1/\Delta_3=513$, $A_1(z=0)=80$ esu, $\Gamma_{ca}=1.3\times10^{10}$ s^{-1}, and $\gamma_c=1.2\times10^8$ s^{-1}, and that the coupling coefficients on line center are given by $\alpha_1=1.03\times10^{-2}$, $\alpha_2=4.29\times10^{-3}$, and $\alpha_3=5.97\times10^{-3}$, which correspond to our experimental conditions. For each case treated we show the spatial evolution of the fields and excited-state population in the box on the left and the spatial evolution of the phases in the box on the right. Figure 6(a) corresponds to the case of perfect phase matching ($\Delta k=0$) and a laser tuned precisely to the two-photon reosnance. The fields rapidly reach their steady-state values and the upper-state population becomes completely suppressed. The effects of increased wave-vector mismatch are shown in Figs. 6(b) and 6(c). For $\Delta k=-30$ cm^{-1} the fields still come rapidly to steady state. However, the steady-state relative phase θ is no longer equal to π, and hence the upper-state population is no longer completely suppressed. For $\Delta k=-100$ cm^{-1}, a steady-state solution to the coupled amplitude equations no longer exists. Physically, this occurs because the nonlinearity is not strong enough to force the various waves to adjust their phases in order to overcome the wave-vector mismatch. Figure 6(d) shows that complete suppression still occurs for the case of a nonzero detuning from the two-photon resonance, although a longer propagation path length is required for the fields to come to steady state.

III. EXPERIMENT

The experiment entails focusing the output of a tunable dye laser into a sodium vapor cell. The dye laser operates at approximately 6855 Å and produces ~500 μJ of energy in a 0.7-cm^{-1} spectral bandwidth in a pulse duration of 1.5—10 ns. The dye laser output is focused to a spot size of ~100 μm in a sodium cell containing between 10^{15} and 10^{17} sodium atoms per cm^3 and ~10 Torr of helium buffer gas. When the laser is tuned to within ~1 Å of the $3s\rightarrow3d$ two-photon transition, a cone of light surrounding the laser beam is emitted in the forward direction, as shown in Fig. 7.[29] In order to determine the spectral composition of this light, the cone is imaged onto the entrance slit of a 0.75-m spectrometer having a resolution of 0.2 Å. The portion of the output spectrum that is near the $3d\rightarrow3p$ transition frequency is shown in Fig. 8(a). The spectrum is seen to be composed of two components due to resonance enhancement by the two fine-structure components of the $3p$ level. Each component extends from resonance to higher frequencies because the phase-matching condition for FWM can be met only for noncollinear propagation for this sign of the detuning.[29] FWM cannot occur in the backward direction because of the large propagation vector mismatch. However, ASE can occur in the backward direction when the laser is tuned to the exact two-photon resonance and when the suppression of the upper-level population is not complete. Figure 8(b) shows the emission spectrum in the backward direction under these conditions. The emission is weak compared to the emission in the forward direction and is seen to consist of two narrow components centered at the two transition frequencies. Figure 8(c) shows the spectrum of the forward emission when the laser is tuned to the exact two-photon resonance. The spectrum is seen to be that of FWM and not of ASE, even though the calculated gain for FWM is much less than that for ASE calculated in the absence of competition. In particular, the gain coefficient for the FWM process is given by $\Lambda^{-1}=33$ cm^{-1} for $N=5\times10^{16}$ cm^{-3} and $A_1=80$ esu. The gain cross section at line center for the $3d\rightarrow3p$ transition under conditions of Doppler broadening is 5×10^{-12} cm^2, and the calculated population inversion ignoring competition effects if 5×10^{15} cm^{-3}, leading to a calculated gain coefficient for ASE of 2.5×10^4 cm^{-1}.

In order to quantify the degree to which FWM suppresses ASE, we have measured the ratio of the emission near the $3d\rightarrow3p$ transition frequency in the backward direction (which is solely ASE) to that in the forward direction (which is due to both ASE and FWM). Shown in Fig. 9 is a plot of this ratio as a function of the peak value of the laser intensity for two different values of the pump beam confocal parameter b. The sodium number density is $\sim1\times10^{16}$ cm^{-3}. It is seen that FWM suppresses ASE more efficiently when the laser intensity and hence the gain for FWM is highest. Since FWM is a phase-matched process, the confocal parameter of the pump laser is an appropriate measure of the effective interaction length. The suppression is also seen to be more complete when the interaction occurs over the longer interaction length that is associated with the use of a larger confocal parameter.

Figure 10 shows the conversion efficiency of the pump wave into the ω_2 wave in both the forward and backward directions as a function of the position of the focus of the incident laser beam relative to the center of the cell.

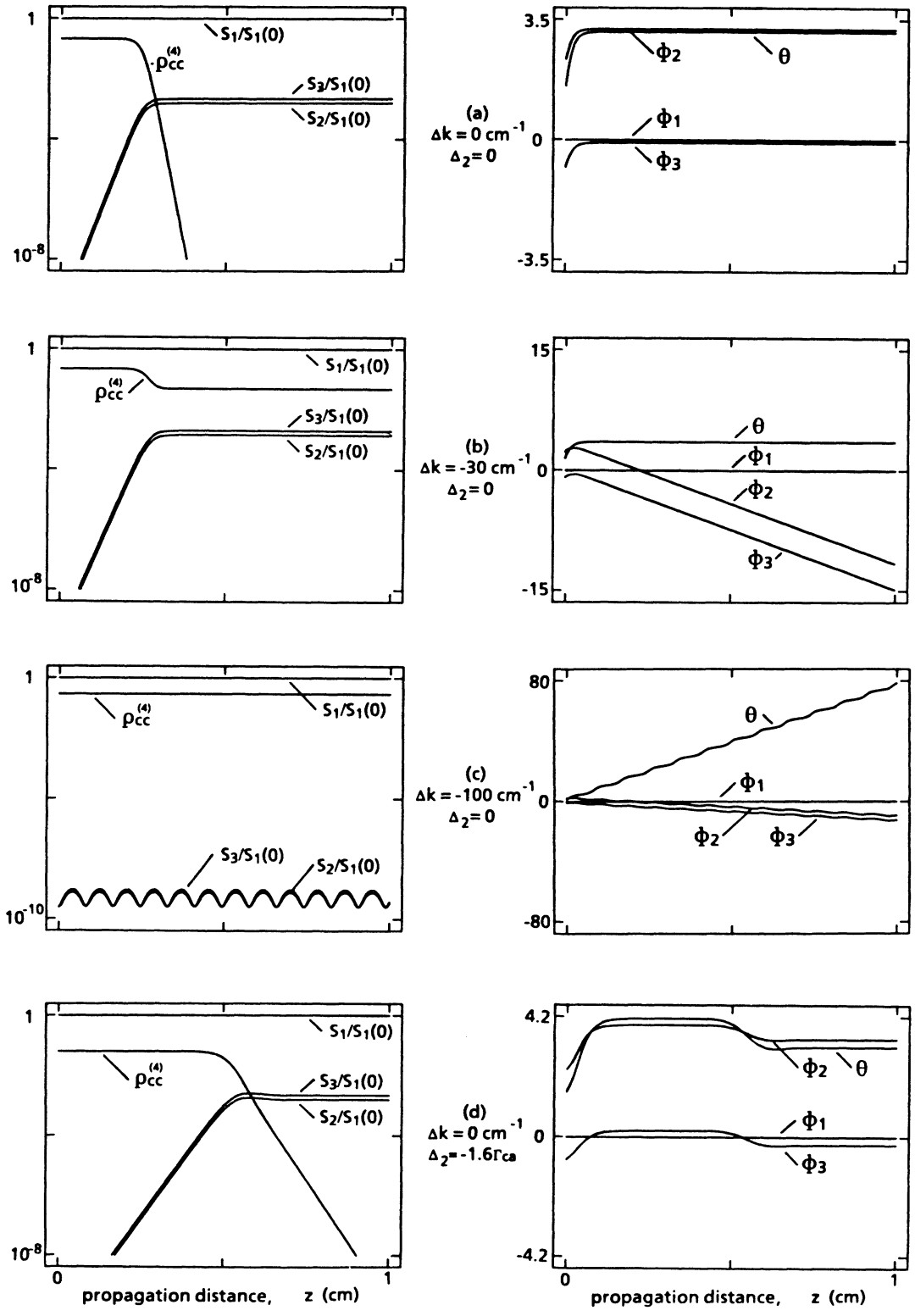

FIG. 6. Spatial evolution of the normalized field intensities S_1, S_2, and S_3, the upper-level population $\rho_{cc}^{(4)}$ (in the left-hand column) and of the phases ϕ_1, ϕ_2, ϕ_3, and θ (given in radians in the right-hand column) for four different cases [(a)—(d)] corresponding to different values of the phase mismatch and detuning from the two-photon resonance. The evolution of the fields is determined by a numerical integration of the coupled amplitude equations (14).

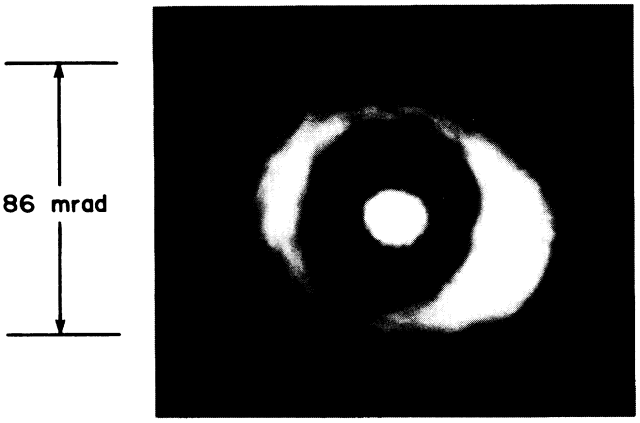

FIG. 7. Transverse intensity profile of the radiation emitted near the $3s \rightarrow 3p$ transition frequency due to FWM for a sodium number density of approximately 5×10^{16} cm^{-3}.

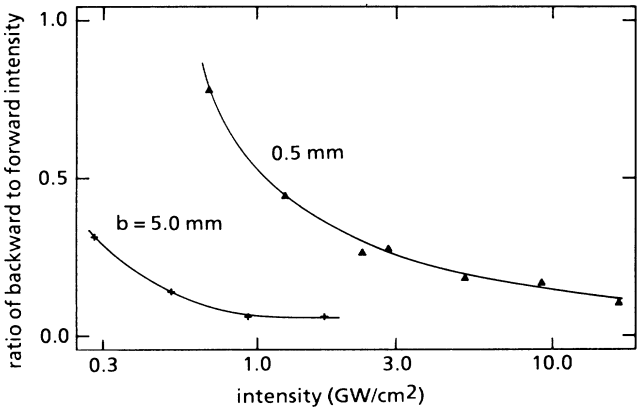

FIG. 9. Ratio of the intensity in the backward direction to that in the forward direction vs incident laser intensity for two different values of the beam confocal parameter. The limiting values of unity and zero correspond to pure ASE and pure FWM, respectively.

These data were collected at a sodium number density of 1×10^{16} cm^{-3}, a confocal parameter of 5 mm, and a peak laser intensity of 400 MW cm^{-3}. Note that the emission into the forward direction is maximized when the focal spot is near the center of the cell. However, the emission into the backward direction (ASE) is suppressed when the position of the focus is near the position that maximizes the forward emission. The dip in the curve is actually shifted slightly toward the entrance face of the cell because under this condition the initiation of the FWM process can occur closer to the entrance face and hence the FWM process can suppress the upper-level population over a greater fraction of the length of the cell.

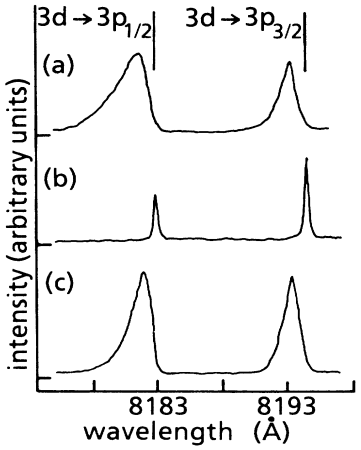

FIG. 8. (a) Spectrum of the radiation generated by FWM in the forward direction for a detuned laser. (b) Spectrum of the radiation (ASE) emitted in the backward direction. (c) Spectrum of the radiation emitted in the forward direction with the laser tuned precisely to the two-photon resonance. Note that this spectrum is that of FWM and not that of ASE.

Figure 11 shows the intensity of the emission at ω_2 in the forward direction as a function of the laser intensity under conditions of strong suppression of ASE. The laser is tuned exactly to the two-photon resonance, and the laser confocal parameter is 5 mm. The intensity of this emission is seen to scale quadratically with the intensity of the input laser, as expected from a FWM process in which the fields have evolved so as to be spatially invariant [see Eq. (27)]. Note that the output intensity depends weakly upon the sodium number density. We believe that this dependence occurs because at higher number densities the conical emission process[29] causes more radiation to be ejected from the interaction region, requiring that more radiation at the ω_2 frequency be generated to maintain the proper amplitude of the ω_2 field within the interaction region.

IV. CONCLUSIONS

In conclusion, we have shown both theoretically and experimentally that four-wave mixing due to the two-

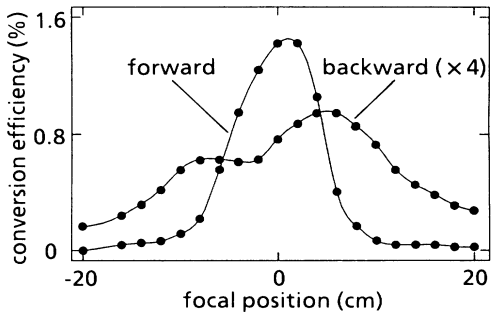

FIG. 10. Intensities of the emission in the forward and backward directions vs position of the beam waist in the cell. Note that ASE is suppressed when FWM is enhanced.

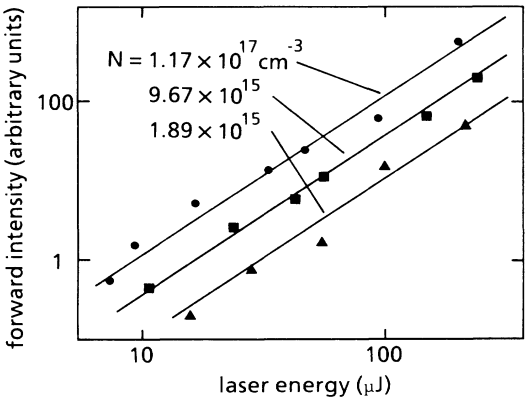

FIG. 11. Intensity of the FWM signal plotted as a function of the laser energy for several different values of the sodium number density. In each case the intensity scales quadratically with the laser energy, as expected on the basis of the model presented in the text.

photon-resonance response of an atomic vapor can lead to the suppression of amplified spontaneous emission from the excited level. The suppression is due to an interference between two excitation pathways connecting the ground and excited states. Under conditions of perfect phase matching, the fields generated by the four-wave-mixing process evolve in such a way that there is complete destructive interference between these two pathways, and hence no population is placed in the upper level. As the wave-vector mismatch is increased, the degree of suppression of the upper-level population becomes less complete. We have observed this suppression experimentally and have shown that the suppression does not occur when the medium is excited by counterpropagating laser beams that cannot efficiently excite the FWM process. We have also conducted a series of experiments that are in agreement with these theoretical predictions in terms of the dependence of the four-wave-mixing efficiency and degree of suppression of the ASE on the pump laser intensity and focusing characteristics.

We acknowledge useful discussions with J. Krasinski and J. J. Wynne. This work was supported by the National Science Foundation Grant No. ECS-8408370 and by the Joint Services Optics Program. In addition, one of us (K.R.) has been supported by the Polish Government Grant No. CPBP01.07.

[1]W. Kaiser and M. Maier, in *Laser Handbook*, edited by F. T. Arecchi and E. O. Schulz-Dubois (North-Holland, Amsterdam, 1972).
[2]J. C. Miller, R. N. Compton, M. G. Payne, and W. R. Garrett, Phys. Rev. Lett. **45**, 114 (1980).
[3]J. H. Glownia and R. K. Sander, Phys. Rev. Lett. **49**, 21 (1982).
[4]D. J. Jackson and J. J. Wynne, Phys. Rev. Lett. **49**, 543 (1982).
[5]J. J. Wynne, Phys. Rev. Lett. **52**, 751 (1984).
[6]D. J. Jackson, J. J. Wynne, and P. H. Kes, Phys. Rev. A **28**, 781 (1983).
[7]M. G. Payne and W. R. Garrett, Phys. Rev. A **26**, 356 (1982).
[8]G. S. Agarwal and S. P. Tewari, Phys. Rev. A **29**, 1922 (1984).
[9]M. S. Malcuit, D. J. Gauthier, and R. W. Boyd, Phys. Rev. Lett. **55**, 1086 (1985).
[10]G. S. Agarwal, Phys. Rev. Lett. **57**, 827 (1986).
[11]D. Grischkowsky, M. M. T. Loy, and P. F. Liao, Phys. Rev. A **12**, 2514 (1975).
[12]Yu. P. Malakyan, Sov. J. Quantum Electron. **15**, 905 (1985).
[13]W. Hartig, Appl. Phys. **15**, 427 (1978).
[14]J. Heinrich and W. Behmenburg, Appl. Phys. **23**, 333 (1980).
[15]P. P. Sorokin, J. J. Wynne, and J. R. Lankard, Appl. Phys. Lett. **22**, 342 (1973).
[16]G. Grynberg, Opt. Commun. **48**, 432 (1984).
[17]G. P. Agrawal, Opt. Commun. **42**, 366 (1982).
[18]R. W. Boyd, D. J. Gauthier, J. Krasinski, and M. S. Malcuit, IEEE J. Quantum Electron. **QE-20**, 1074 (1984).
[19]J. Bokor, R. R. Freeman, R. L. Panock, and J. C. White, Opt. Lett. **6**, 182 (1981).
[20]T. Y. Fu and M. Sargent III, Opt. Lett. **5**, 433 (1980).
[21]R. T. Hodgson, P. P. Sorokin, and J. J. Wynne, Phys. Rev. Lett. **32**, 342 (1972).
[22]R. R. Freeman, G. C. Bjorklund, N. P. Economou, P. F. Liao, and J. E. Bjorkholm, Appl. Phys. Lett. **33**, 739 (1978).
[23]L. Allen and G. I. Peters, Phys. Rev. A **8**, 2031 (1973).
[24]J. Okada, K. Ikeda, and M. Matsuoka, Opt. Commun. **26**, 189 (1978).
[25]E. A. Manykin and A. M. Afanas'ev, Zh. Eksp. Teor. Fiz. **52**, 1246 (1967) [Sov. Phys.—JETP **25**, 828 (1967)]; H. Kildal and S. R. J. Brueck, IEEE J. Quantum Electron. **QE-16**, 566 (1980); V. V. Krasnikov, M. S. Pshenichnikov, and V. S. Solomatin, Pis'ma Zh. Eksp. Teor. Fiz. **43**, 115 (1986) [JETP Lett. **43**, 148 (1986)].
[26]R. R. Freeman, J. Bokor, and W. E. Cooke, Phys. Rev. A **26**, 3029 (1982).
[27]R. Karplus and J. Schwinger, Phys. Rev. **73**, 1020 (1948).
[28]N. Bloembergen and Y. R. Shen, Phys. Rev. **133**, A37 (1964).
[29]J. Krasinski, D. J. Gauthier, M. S. Malcuit, and R. W. Boyd, Opt. Commun. **54**, 241 (1985).

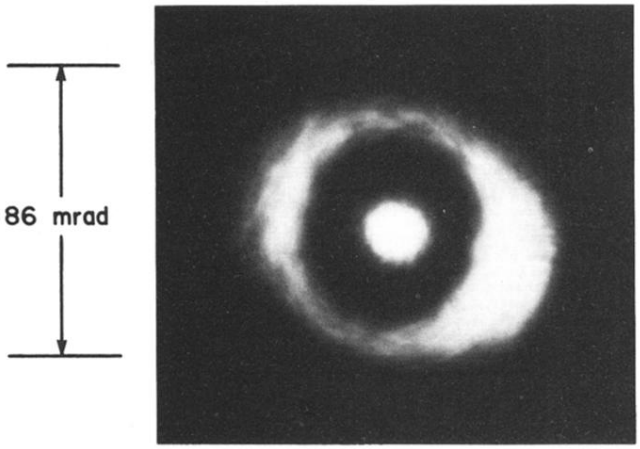

FIG. 7. Transverse intensity profile of the radiation emitted near the $3s \rightarrow 3p$ transition frequency due to FWM for a sodium number density of approximately 5×10^{16} cm^{-3}.